Journal of Computational Neuroscience 17, 203–223, 2004

Oscillations in Large-Scale Cortical Networks: Map-Based Model

N.F. RULKOV
Institute for Nonlinear Science, University of California, San Diego, La Jolla, CA 92093, USA

I. TIMOFEEV
Laboratory of Neurophysiology, School of Medicine, Laval University, Quebec, Canada G1K 7P4

M. BAZHENOV
The Salk Institute, Computational Neurobiology Laboratory, La Jolla, CA 92037, USA
bazhenov@salk.edu

Received February 20, 2004; Revised April 27, 2004; Accepted June 10, 2004

Action Editor: David Golomb

Abstract. We develop a new computationally efficient approach for the analysis of complex large-scale neurobiological networks. Its key element is the use of a new phenomenological model of a neuron capable of replicating important spike pattern characteristics and designed in the form of a system of difference equations (a map). We developed a set of map-based models that replicate spiking activity of cortical fast spiking, regular spiking and intrinsically bursting neurons. Interconnected with synaptic currents these model neurons demonstrated responses very similar to those found with Hodgkin-Huxley models and in experiments. We illustrate the efficacy of this approach in simulations of one- and two-dimensional cortical network models consisting of regular spiking neurons and fast spiking interneurons to model sleep and activated states of the thalamocortical system. Our study suggests that map-based models can be widely used for large-scale simulations and that such models are especially useful for tasks where the modeling of specific firing patterns of different cell classes is important.

Keywords: slow-wave sleep, waking, cortex, difference equation, large-scale network model

Introduction

Brain systems consist of a large number of various types of neurons interconnected with electrical and chemical synapses of different polarity. To study the functionality of a brain system, modeling of large-scale networks, containing hundreds of thousands of neurons, is needed. Computer models commonly used for neurobiological simulations are based on dynamical systems given by *ordinary differential equations* (ODE). To describe the dynamics of firing patterns generated by a neuron, such models should contain variables of multiple time scales ranging from less than one millisecond (to control spike generation) to hundreds of milliseconds to describe slow intrinsic and synaptic processes. Such a diversity of time scales limits the speed of the numerical simulations.

We propose a way to improve computational efficiency of network simulations by designing a model that ignores the duration and shape of individual spikes, but captures the dynamics of the other time scales. This is achieved by using a dynamical system written in the form of *difference equations* (a map) that generate a sequence of membrane potential samples in discrete

moments of time. In this approach each spike takes only one sample in the waveform data. The other, relatively slow dynamical processes imprinted in the firing pattern can be captured correctly, because the discreteness of time does not alter their relatively slow dynamics. An example of such a map-based model has been recently proposed for modeling of spiking-bursting neuron activity (Rulkov, 2002). Attractive features of this map-based model include the simplicity of the equation, the ability to describe a broad range of firing patterns found in biological neurons (Jahnsen and Llinás, 1984; McCormick et al., 1985; Connors and Gutnick, 1990; Gray and McCormick, 1996; Steriade et al., 1998), and the possibility to adopt models of synapses typically used in simulations of networks with Hodgkin-Huxley (HH) equations.

In this paper we develop a map-based model approach for numerical simulations of large-scale cortical networks. Specific applications reported in the paper include the following: simple and computationally efficient map-based models that reproduce the electrophysiological fingerprints of cortical neurons are proposed; it is shown that for one–dimensional networks map-based models yield results similar to those obtained with HH neurons; multi-dimensional multilayer networks of map-based neurons can be simulated using conventional workstations; in contrast to non-spiking models of neurons (e.g. firing-rate models) map-based models can produce information about oscillations, synchronization and correlations. Using two-dimensional network simulations with up to 100,000 neurons we explored regimes of self-sustained neuronal activity in the form of interacting rotating spiral waves. The dynamical features of this activity was very similar to slow-wave sleep (SWS) oscillations—low-frequency (0.3–1 Hz) rhythms dominating cortical activity during natural sleep and under some types of anesthesia (Steriade et al., 1993a, 1993b, 2001; Timofeev et al., 2001b). Transitions between the state composed of slow waves and the activated state (which is reminiscent of awake like activity) were modeled by changing intrinsic parameters of the model neurons.

Materials and Methods

In vivo Recordings

Experiments were carried out on adult cats anesthetized with sodium pentobarbital (commercial name SOMNATOL, 35 mg/kg, i.p.; $n = 37$). The electroencephalogram (EEG) was monitored continuously during the experiments to ascertain the depth of anesthesia. Additional doses of the same anesthetic were given at the slightest tendency toward activated EEG patterns. The tissue to be incised and the pressure points were infiltrated with lidocaine (2%). The cats were paralyzed with gallamine triethiodide only after the EEG showed typical signs of deep general anesthesia and were ventilated artificially with the control end-tidal CO_2 at 3.5–3.8%. The rectal temperature was monitored and maintained at 37–38°C and the heart rate was 90–110 beats/min. The stability of intracellular recordings was ensured by bilateral pneumothorax, cisternal drainage, hip suspension, and by filling holes that were opened in the cranium with a warm agar (4% in 0.9% saline). At the end of experiments, the animals were given a lethal dose of pentobarbital (50 mg/kg i.v.). The experimental protocol has been approved by the committee for animal care in Laval University and also confirms with guidelines recommended by the National Institute of Health.

Intracellular recordings of cortical neurons from areas 5 and 7 were performed with glass micropipettes filled with a solution of 3 M potassium acetate. The electrode had a DC resistance of 30–80 MΩ. A high-impedance amplifier (bandpass, 10 kHz) with an active bridge circuitry was used to record and inject currents into the cells. All electrical signals were digitized online with a sampling rate of 20 kHz.

Hodgkin-Huxley Type Model

Intrinsic Currents. The cortical pyramidal (PY) cells and interneurons (INs) were modeled with two-compartment models with channels described by Hodgkin-Huxley kinetics (Mainen and Sejnowski, 1996):

$$C_m \frac{dV_D}{dt} = -g_L(V_D - E_L) - g(V_D - V_S) - I_D^{\text{int}} - I^{\text{syn}},$$
$$g(V_S - V_D) = -I_S^{\text{int}}, \quad (1)$$

where C_m, g_L are the membrane capacitance and the leakage conductance of the dendritic compartment, E_L is the reversal potential, V_D and V_S are the membrane potentials of dendritic and axo-somatic compartments, I_D^{int} and I_S^{int} are a sums of active intrinsic currents in axo-somatic and dendritic compartments, I^{syn} is a sum of synaptic currents and g is the conductance between axo-somatic and dendritic compartments. In this

model, the axo-somatic compartment had no capacitance, which sped up the simulations but had little effect on the spike firing patterns (Mainen and Sejnowski, 1996). The soma and axon initial segment is characterized by high conductance densities; when capacitance is included in this compartment smaller integration steps were needed to ensure stability of the calculation, but model firing patterns were unaffected (Mainen and Sejnowski, 1996). The model includes a high density of fast Na^+ channels in the axo-somatic compartment and a low density in the dendritic compartment. A fast potassium current is present in the axo-somatic compartment. A slow voltage-dependent K^+ M-current, slow Ca^{2+} dependent K^+ current, a high-threshold Ca^{2+} current, persistent Na^+ current, a hyperpolarization-activated cation current (h-current) and a potassium leak current, $I_{KL} = g_{KL}(V - E_{KL})$, were included in the dendritic compartment. The expressions for the voltage- and Ca^{2+}-dependent transition rates for all currents are given in Timofeev et al. (2000). The maximal conductances and passive properties were $S_{soma} = 1.0 \cdot 10^{-6}$ cm^2, $g_{Na} = 3000$ mS/cm^2, $g_K = 200$ mS/cm^2 for the axo-somatic compartment and $C_m = 0.75$ μF/cm^2, $g_L = 0.033$ mS/cm^2, $g_{KL} = 0 - 0.0025$ mS/cm^2, $S_{dend} = S_{soma}r$, $g_{Ca} = 0.01$ mS/cm^2, $g_{Na} = 1.5$ mS/cm^2, $g_{KCa} = 0.3$ mS/cm^2, $g_{Km} = 0.01$ mS/cm^2, $g_{Na(p)} = 0.02-0.046$ mS/cm^2 for the dendritic compartment. $E_L = -68$ mV and $E_{KL} = -95$ mV. No $I_{Na(p)}$ was modeled for IN cells. The resistance between compartments was $R = 10$ MΩ.

The firing properties of the model in Eq. (1) depend on the coupling conductance between compartments ($g = 1/R$) and the ratio of dendritic area to axo-somatic area r (Mainen and Sejnowski, 1996). Such dependence of the firing properties in two-compartmental neuron model on the electrical coupling between compartments was first described in Pinsky and Rinzel (1994). In the network simulations, we used a model of a regular-spiking neuron for PY cells ($r = 140$) and a model of a fast spiking neuron for IN cells ($r = 50$).

Synaptic Currents. All synaptic currents were calculated according to:

$$I_{syn} = g_{syn}[O](V - E_{syn}), \tag{2}$$

where g_{syn} is the maximal conductivity, $[O](t)$ is the fraction of open channels and E_{syn} is the reversal potential. $E^{syn}_{AMPA} = 0$ mV for AMPA receptors and $E^{syn}_{GABAA} = -70$ mV for $GABA_A$ receptors. A simple phenomenological model was used to describe short-term depression of intracortical excitatory connections (Abbott et al., 1997; Tsodyks and Markram, 1997; Galarreta and Hestrin, 1998; Timofeev et al., 2000). According to this model a maximal synaptic conductance was multiplied with a depression variable, $D \leq 1$, representing the amount of available "synaptic resources". $D = 1-(1-D_i(1-U))\exp(-(t-t_i)/\tau)$, where $U = 0.07$ is the fraction of resources used per action potential, $\tau = 700$ ms the time constant of recovery of the synaptic resources, D_i the value of D immediately before the ith event, and $(t - t_i)$ the time after the ith event.

$GABA_A$ and AMPA synaptic currents were modeled by first-order activation schemes (Destexhe et al., 1994b). The equations for all synaptic currents are given in Timofeev et al. (2000). The maximal conductances (for each synapse) were $g_{AMPA(PY-PY)} = 0.08$–$0.15\,\mu$S, $g_{AMPA(PY-IN)} = 0.05\,\mu$S and $g_{GABA_A(IN-PY)} = 0.05\,\mu$S.

Computational Map-Based Model

Base Model. To model the dynamics of large-scale networks we used a computationally efficient phenomenological model implemented in the form of difference equations (a map). This map-based model is capable of generating various types of spiking and spiking-bursting activity and in its original form is written as Rulkov (2002)

$$\begin{aligned} x_{n+1} &= f_\alpha(x_n, x_{n-1}, y_n + \beta_n), \\ y_{n+1} &= y_n - \mu(x_n + 1) + \mu\sigma + \mu\sigma_n, \end{aligned} \tag{3}$$

where x_n is the fast and y_n is the slow dynamical variable. Slow time evolution of y_n is achieved by using small values of the parameter $0 < \mu \ll 1$. Parameters α and σ control the dynamics and they are set to mimic the behavior of a particular type of neuron. Input variables β_n and σ_n incorporate the action of synaptic inputs I^{syn} and also the action of some intrinsic currents that are not explicitly captured by model (3). The nonlinear function $f_\alpha(x_n, x_{n-1}, y_n + \beta_n)$ is given by

$$\begin{aligned} &f_\alpha(x_n, x_{n-1}, u) \\ &= \begin{cases} \alpha/(1 - x_n) + u, & x_n \leq 0 \\ \alpha + u, & 0 < x_n < \alpha + u \text{ and } x_{n-1} \leq 0 \\ -1, & x_n \geq \alpha + u \text{ or } x_{n-1} > 0, \end{cases} \end{aligned} \tag{4}$$

where $u = y_n + \beta_n$. Such a form of nonlinearity was proposed in Rulkov (2002) to achieve the birth of a limit cycle whose waveform appear as a sequence of sharp spikes. Each of these spikes is formed using only one sample which occurs on the top of the spike. This sample corresponds to the trajectory point occurred on the rightmost interval of the function. As the result our map-based model uses only one iteration to form a spike and never misses a spike. To ensure that, after being perturbed by various types of inputs, the map still reliably produces sharp spikes with only one point on the top of each spike the nonlinear function (5) adopts a modification (dependence on x_{n-1}), which was suggested and discussed in detail in the last section of Rulkov (2002).

The individual dynamics of the fast subsystem, given by the first equation of (3) with $y_n = y^{rs} = \text{const}$, $\beta_n = 0$, is designed in such a way that it can replicate the states of silence or tonic spiking depending on the value of the control parameters α and y^{rs}. Comparison of the dynamics of the fast subsystem with the dynamics of a minimal model based on Hodgkin-Huxley kinetics shows that this subsystem is sufficient to replicate the membrane potential dynamics caused by a transient sodium current, I_{Na}, and a fast potassium current, I_{K}. The values of x_n can be rescaled to have correct voltage units that represent the membrane potential measured in experiments. However, we do not rescale the variable x_n in this paper for the sake of simplicity and computational efficiency.

The second equation of (3) introduces slow transient dynamics between the two states of the fast subsystem and is used to capture various effects such as spike adaptation and the generation of bursts of spikes. Although the slow subsystem in (3) is not derived from any biological framework it still can be designed in such a way that the map-based model can mimic prevalent electrophysiological characteristics of neurons caused by biological processes. Depending on the values of σ and α the individual dynamics of the basic model ($\beta_n = 0$ and $\sigma_n = 0$) show the following types of behavior, which can be easily understood using the analysis of a phase portrait (see Rulkov, 2002; Shilnikov and Rulkov, 2003). When $\sigma < \sigma_{th} = 2 - \sqrt{\alpha/(1-\mu)}$ the system converges to the stable fixed point O_0 with the coordinates $x_O = -1 + \sigma$ and $y_O = -1 + \sigma - \alpha/(2-\sigma)$ and stays silent. At the threshold $\sigma = \sigma_{th}$ the fixed point loses stability due to a subcritical Andronov-Hopf bifurcation and, for $\sigma > \sigma_{\text{th}}$ the map generates continuous spikes or bursts of spikes depending on the value of α.

The design of model (3) relies on the bifurcation methodologies and in that sense is similar to a model recently proposed by Izhikevich (2003), which is designed in the form a two-dimensional system of ordinary differential equations. Integrating Izhikevich's model using a large step Euler scheme one transforms the ODE system into a two-dimensional map. The dynamics of such a map and our model are similar and both maps allow replicating a large variety of firing patterns. It is shown in Izhikevich (2004) that this type of models is more efficient, in terms of simulation speed with a potential to generate realistic firing patterns of various types of neurons, than most other simple ODE-based models including well-known integrate-and-fire model. The main differences between the map-based model proposed in this manuscript and Izhikevich's model is that our design is based directly on the map dynamics and the map is designed to ensure that no spikes are missing and that each spike is formed with the minimal number of steps (iterations). Map-based model always generates a sample on the top of each spike. In the case of Izhikevich's model the dynamical properties of the model are designed within a framework of continuous time system and it is unclear if these properties remain when one uses a large step Euler integration scheme that gives only one or two steps within the width of spike.

Considering map (3) in the parameter region $\alpha < 4$ we omit the regimes of spiking-bursting activity in the individual dynamics of the basic model and allow the model to generate activity only in the form of tonic spiking or silence, see Rulkov (2002) for details. The type and characteristics of the selected behavior are controlled by parameter σ which sets the baseline level of the cell. Consider the case when the baseline level is set in the silence mode. The system can be excited by a rectangular pulse of depolarizing current $I_n = A$, for $n_{\text{start}} \le n \le n_{\text{end}}$, and $I_n = 0$, otherwise. Acting through the input variable σ_n, $\sigma_n = \sigma^e I_n$, the current pushes the system over the excitation threshold σ_{th} and the map generate spikes during the action of the pulse. Figure 1 shows firing patterns induced by such a pulse. Consecutive iterations of x_n in the two top plots are connected with straight lines. Such lines will be used throughout the paper to present the firing patterns of neurons while the actual values of x_n shown by small black circles will be omitted. Note that the input variable σ_n acts as a variation of parameter

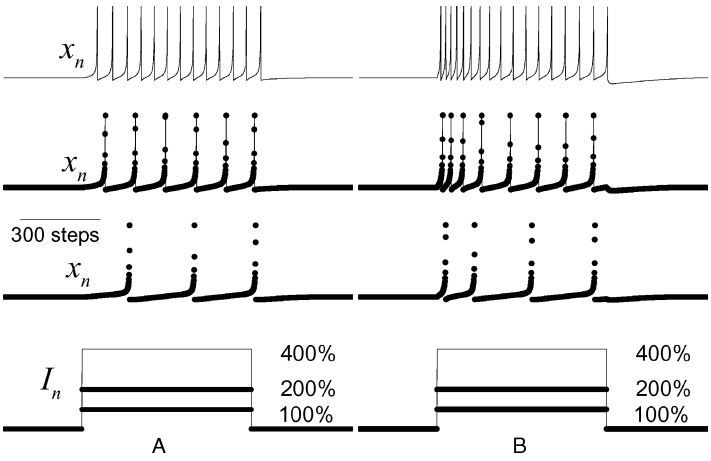

Figure 1. Waveforms of x_n illustrating the role of the parameter β^e in the generation of firing responses of the map model (3). A rectangular pulse of an external depolarizing current I_n of duration 870 iterations and amplitude A, $2A$ (200%) and $4A$ (400%) was applied to excite the activity. The parameter values are: $\alpha = 3.65, \sigma = 6.0\text{E}{-2}, \mu = 0.0005, \sigma^e = 1.0$, and $A = 3.1\text{E}{-2}$. (A) shows the case $\beta^e = 0.0$ and (B) $\beta^e = 0.133$. The actual values of x_n and I_n from (3) are shown with small black circles for the cases of 100% and 200% of the pulse amplitude. The iterations of x_n in the top plots are connected with lines (cases of 200% and 400%).

σ (see Eq. (3)). The frequency of spiking increases as the level of depolarization (amplitude A) is increased (Fig. 1).

Capturing the Effects Associated with Other Ionic Currents. In our study the base model will be supplemented with an input variable β_n that, as well as the input variable σ_n, will be a function of the synaptic currents. The role of β_n becomes clear when one examines the reaction of the model to a rectangular pulse I_n. Setting this input parameter to be proportional I_n, namely, $\beta_n = \beta^e I_n$, one can replicate the effects of deceleration of spiking (spike frequency adaptation) and afterhyperpolarization. The model map reacts to the changes of β_n instantly. It is equivalent to a fast shift of the value of the slow variable y_n by the value $\beta_n - \beta_{n-1}$ which makes the fast map (3) start spiking instantly at a fast rate. Then, if β_n does not change, the state of the map slowly drifts back as the variable y_n changes. The rate of this drift is controlled by parameter μ. Typical patterns generated by the model with this setting are shown in Fig. 1B. This dynamical mechanism allows us to replicate the effects of spiking deceleration and afterhyperpolarization, without increasing the number of equations in the model. We use this approach to replicate the properties of regular spiking cells.

To control the effect of hyperpolarization caused by each generated spike, we modify the model (3) in the following way. We introduce a phenomenological hyperpolarizing current I_n^{hp} generated by the action of each spike,

$$I_{n+1}^{hp} = \gamma^{hp} I_n^{hp} - \begin{cases} g^{hp}, & \text{if the } n\text{-th iteration} \\ & \text{carries a spike} \\ 0, & \text{otherwise.} \end{cases} \quad (5)$$

Parameter γ^{hp} controls the duration, $\tau^{hp} \sim (1 - \gamma^{hp})^{-1}$, and parameter g^{hp} the amplitude of the hyperpolarizing current. In accordance with Eq. (4) the first condition in (5) is satisfied only when $x_n \geq \alpha + y_n + \beta_n$ or $x_{n-1} > 0$. Equation (5) substitutes the slow subsystem of the base model (3). The fast subsystem in this case can be written in the following form

$$x_{n+1} = f_\alpha\big(x_n, x_{n-1}, y^{rs} + \beta^{hp} I_n^{hp} + \beta^e I_n\big), \quad (6)$$

where y^{rs} is a constant defining the resting state of the modified model. Here, the slow variable I_n^{hp} is computed with (5). The effects of after-spike hyperpolarization captured by this model are illustrated in Fig. 2 where a depolarizing rectangular pulse of external current I_n excites the cell. When a spike is generated, it excites an I^{hp} pulse which hyperpolarizes the cell, see the x_n waveforms. The depth and duration of the hyperpolarization is controlled by parameter g^{hp} and γ^{hp} respectively (Fig. 2). Equations (5), (6) are used for the description of the interneuron (IN) dynamics.

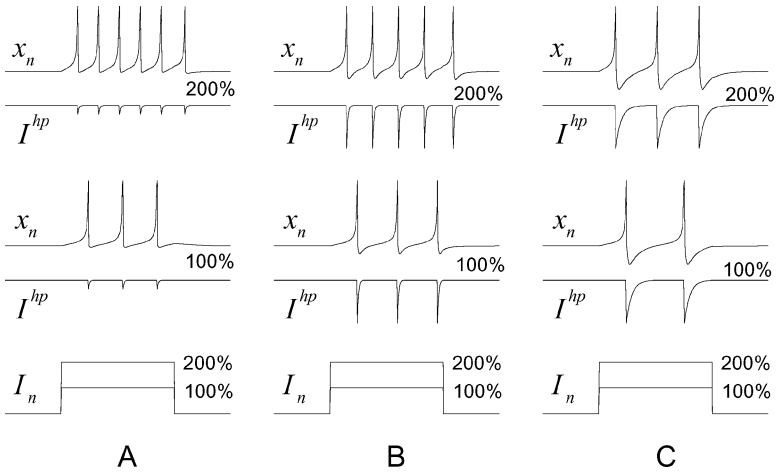

Figure 2. Modeling the effect of hyperpolarization after a spike with the map-based neurons given by Eqs. (5) and (6). The fixed parameters are $\alpha = 3.8$, $\mu = 0.002$, $y^{rs} = -2.9$, $\beta^{hp} = 0.5$, $\beta^{e} = 0.1$ and the duration of depolarizing pulse -200 iterations. The parameters γ^{hp}, g^{hp} and the pulse amplitude A are varied to illustrate the role of these parameters. 100% corresponds to $A = 0.5$. The three cases A, B and C correspond to $\gamma^{hp} = 0.6$, $g^{hp} = 0.1$; $\gamma^{hp} = 0.6$, $g^{hp} = 0.5$; $\gamma^{hp} = 0.9$, $g^{hp} = 0.5$, respectively.

Modeling of Synaptic Inputs. In the case of map-based models, the equation for synaptic currents can be adopted from the known ODE models used in HH-type simulations, but they need to be rewritten in the form of difference equations. The simplest map-based model for a synaptic current can be written as

$$I^{\text{syn}}_{n+1} = \gamma I^{\text{syn}}_{n} - \begin{cases} g_{\text{syn}}\left(x^{\text{post}}_{n} - x_{rp}\right), & \text{spike}_{\text{pre}}, \\ 0, & \text{otherwise}, \end{cases} \tag{7}$$

where g_{syn} is the strength of synaptic coupling, indexes *pre* and *post* stand for the presynaptic and postsynaptic variables, respectively. The first condition, "$\text{spike}_{\text{pre}}$", is satisfied when $x^{\text{pre}}_{n} \geq \alpha + y^{\text{pre}}_{n} + \beta^{\text{pre}}_{n}$ or $x^{\text{pre}}_{n-1} > 0$, i.e. when the value x^{pre}_{n} is in the right-most interval of function (4). It corresponds to the moments of time when presynaptic spikes are generated. Parameter γ in (7) controls the relaxation rate of synaptic ($0 \leq \gamma < 1$). Parameter x_{rp} defines the reversal potential and, therefore, the type of synapse: excitatory or inhibitory. To model a synaptic delay, the implementation of condition "$\text{spike}_{\text{pre}}$" in (7) is delayed from the moment of the presynaptic spike generation by the number of iterations corresponding to the delay time. In this paper such a delay is not used unless it is specified.

The effect of short-term depression in the synapse can be achieved by supplementing Eq. (7) with an additional variable d_n that controls the strength of the coupling. In this case I^{syn}_{n} can be computed with a system of two difference equations for the variables $\{I^{\text{syn}}_{n}, d_n\}$ given in the following form

$$\left\{I^{\text{syn}}_{n+1}, d_{n+1}\right\} = \begin{cases} \left\{\gamma I^{\text{syn}}_{n} - g_{\text{syn}} d_n \left(x^{\text{post}}_{n} - x_{rp}\right), (1-\eta) d_n\right\}, & \text{spike}_{\text{pre}}, \\ \left\{\gamma I^{\text{syn}}_{n}, 1 - (1-\rho)(1-d_n)\right\}, & \text{otherwise}, \end{cases} \tag{8}$$

where $0 \leq \eta < 1$ controls the depression rate by fading the synapse strength each time a presynaptic spike is received, and $0 < \rho \ll 1$ controls the rate of synapse strength recovery. The initial conditions here are $\{I^{\text{syn}}_{0}, d_0\} = \{0, 1\}$.

Operating in the network each cell receives many synaptic inputs. Modeling the network we normalize the strength of each synaptic coupling g_{syn} by the number of synaptic inputs of the same type (inhibitory or excitatory). We also limit the range of values in the portion of β_n representing the total synaptic currents. This range is set to $(-0.0001, 0.1)$ in order to ensure the robustness of the computational scheme.

Network Geometry

Both one-dimensional and two-dimensional network models are considered. The cortical model consisted of a two-layer array of N PY and M IN cells, as described in our previous studies (see, e.g. Bazhenov

et al., 2002). The network geometry in the simulations with HH neurons and map-based models were the same. In the HH simulations N was varied between 64 and 512, and M between 16 and 128. In map-based simulations we considered similar networks where N and M were limited to 262144 and 65536, respectively. In one-dimensional simulations the connection fan out was varied between ± 8 and ± 32 cells for AMPA mediated PY-PY synapses; between ± 8 and ± 32 cells for AMPA mediated PY-IN synapses; between ± 2 and ± 8 cells cells for $GABA_A$ mediated IN-PY synapses. The radii of the connection footprints are noted as L_{PY-PY}, L_{PY-IN}, and L_{IN-PY}, respectively. In two-dimensional models the radius of connection fan out was 8 neurons ($\sim$200 presynaptic neurons) for AMPA mediated PY-PY synapses; 8 ($\sim$200 presynaptic neurons) neurons for AMPA mediated PY-IN synapses; 2 ($\sim$12 presynaptic neurons) neurons for $GABA_A$ mediated IN-PY synapses.

Data Analysis

The cross-correlation of the neuronal firing at spatially separated network spots was computed as

$$C(t_d, k, l, k', l') = \frac{\sum_n \left(x_n^s(k,l) - \overline{x_n^s(k,l)}\right)\left(x_{n+t_d}^s(k',l') - \overline{x_{n+t_d}^s(k',l')}\right)}{\sum_n \left(x_n^s(k,l) - \overline{x_n^s(k,l)}\right)^2} \tag{9}$$

where (k, l) and (k', l') are the indexes of cells located in the center of the spots, $\overline{x_n^s(k,l)} = \sum_{n=1}^{N}(x_n^s(k,l)/N)$, and N is the number of data point of x_n^s used for the analysis.

Computational Methods

All simulations with HH model neurons described in the paper were performed using fourth-order Runge-Kutta (RK(4)) method and in some cases embedded Runge-Kutta (RK6(5)) method with time step 0.02 ms.

Results

Response Patterns of Individual Neurons

We developed map-based models capable of replicating the spiking activity observed in different types of cortical pyramidal (PY) neurons and interneurons (INs). Three common types of intrinsic neuronal firing patterns of cortical neurons were studied: fast-spiking (FS), regular-spiking (RS) and intrinsically-bursting (IB). Figure 3 compares the intrinsic neuronal discharges found *in vivo* (Fig. 3A), simulated with a Hodgkin-Huxley model (Fig. 3B) and with map-based models (Fig. 3C). A FS neuron (Fig. 3, left) is characterized by constant spiking frequency without spike frequency adaptation over the duration of a DC pulse. A RS neuron (Fig. 3, middle) displayed an initial higher frequency response followed by spike frequency adaptation controlled by the activation of a Ca^{2+} dependent K^+ current. An IB neuron (Fig. 3, right panels) responded with a burst of spikes at the very beginning of DC stimulation followed by non-adaptive spiking. This burst is a result of the activation of high-threshold Ca^{2+} and persistent Na^+ currents.

These three common patterns of firing can be replicated by means of map-based models. The left panel of Fig. 3C shows the firing patterns produced by model (5) and (6) when the map is driven by I_n. The parameters of the model were set to obtain realistic shapes of the firing patterns generated by the FS cell for various levels of the input pulse I_n.

The middle and right panels of Fig. 3C show the firing patterns generated by model (3). Deceleration of spikes in this case was achieved by means of the parameter β^e which controls the dynamics of the transients. The model parameters were set to reproduce spike frequency adaptation and afterhyperpolarization in RS and IB neurons found *in vivo* and replicated with the corresponding Hodgkin-Huxley models. Comparing the time characteristics of patterns in the HH models and the map-based models for these parameter settings we estimated that *one iteration* of the map corresponds approximately to 0.5 msec of time in the HH model. This estimation has been used throughout the manuscript to set a time scale for the map-based models.

An increase in the amplitude of the depolarizing current increased the firing rate of the studied neurons. The dependency of spiking frequency on the values of the external DC current I_n was used to set correct time characteristics of the map-based models. This dependency computed for the RS and FS cells is shown in Fig. 4. These plots were obtained for the models with small noise r_n, uniformly distributed in the interval $(-0.01, 0.01)$, added to the equations of x_n in both models ($x_{n+1} = f_\alpha(\cdots) + r_n$, see (3) and (6) for

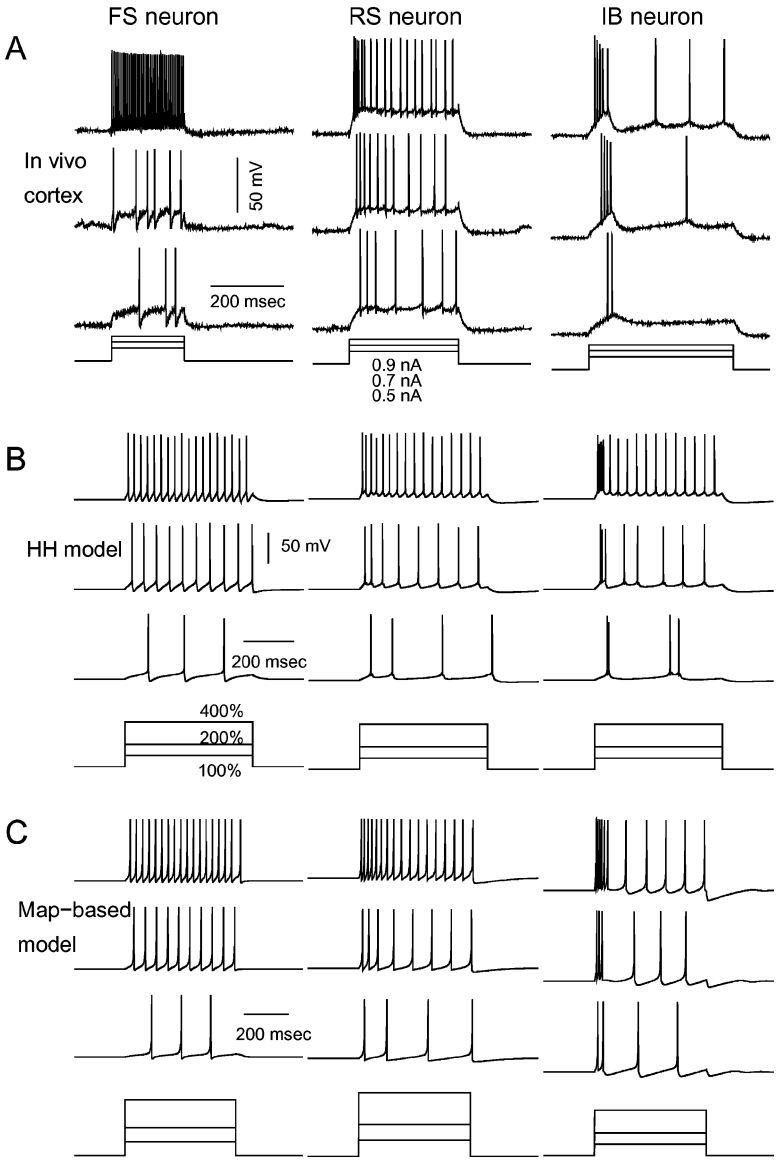

Figure 3. Intrinsic neuronal firing patterns *in vivo* and in the models. (A) *In vivo* data. (B) Hodgkin-Huxley model. (C) Map-based model. Left panels show a fast spiking (FS) neuron; middle panel—regular spiking (RS) neuron; right panel—intrinsically bursting (IB) neuron. The HH model is given by (1) with $g_{\mathrm{Na}(p)} = 0.02$ mS/cm^2, $g_{\mathrm{Ca}} = 0.01$ mS/cm^2 for the FS neuron; $g_{\mathrm{Na}(p)} = 0.046$ mS/cm^2, $g_{\mathrm{Ca}} = 0.035$ mS/cm^2, $r = 140$ for the RS neuron; and $g_{\mathrm{Na}(p)} = 0.046$ mS/cm^2, $g_{\mathrm{Ca}} = 0.035$ mS/cm^2, $r = 150$ for the IB neuron. The map-based model of the FS cell is given by (5) and (6) with $\alpha = 3.8$, $y^{rs} = -2.9$, $\beta^{hp} = 0.5$, $\gamma^{hp} = 0.6$, $g^{hp} = 0.1$, $\beta^{e} = 0.1$, and amplitude of rectangular pulse $A = 1.6$E–2 (100%). The map-based models of the RS and the IB cell are given by (3), where $\alpha = 3.65$, $\sigma = 6.0$E–2, $\mu = 0.0005$, $\sigma^{e} = 1.0$, $\beta^{(e)} = 0.133$, and $A = 3.0$E–2 for the RS cell; and $\alpha = 4.1$, $\sigma = -3.6$E–2, $\mu = 0.001$, $\sigma^{e} = 1.0$, $\beta^{(e)} = 0.1$, and $A = 1.0$E–2 for the IB cell. The duration of the depolarizing pulse in the map-based simulation is 870 iterations, which is approximately 430 msec.

details). This additional noise was important to show that the characteristics of the model are robust. It also eliminated the fine staircase structure of the plots that occurred due to discrete values of inter-spike intervals in the map at fast firing rates. The firing rate of the RS neuron was calculated based on the steady-state (after adaptation is completed) phase of the response. Our results are in good agreement with experimental data (see, e.g., Fig. 6 in McCormick et al. (1985) and Figs. 8 and 9 in Mason and Larkman (1990)). A role of spike

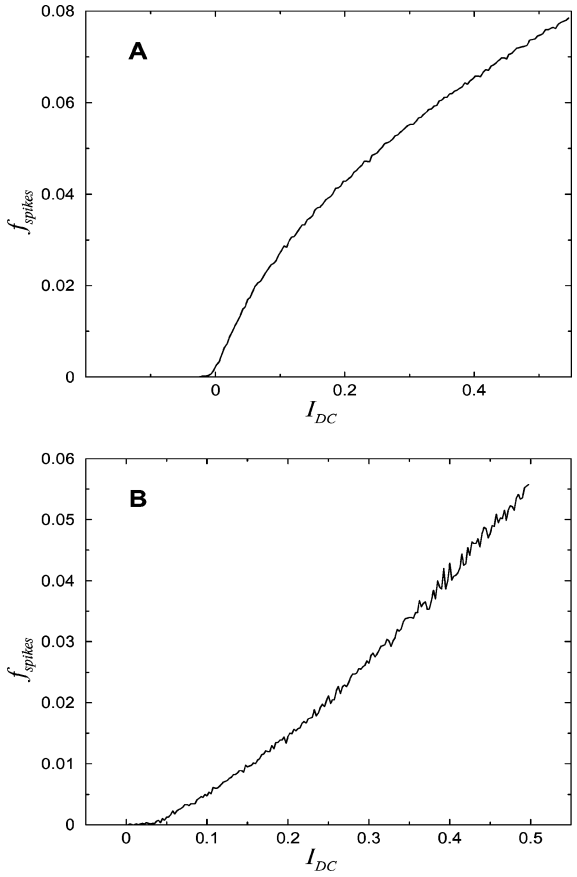

Figure 4. Dependence of firing rate f_{spikes} on the level of depolarizing current $I_n = I_{\text{DC}}$ computed for the FS cell—panel (a) and the RS cell—panel (b). The parameters of the maps are the same as in Fig. 3. In (a) the solid line corresponds to the case $g^{hp} = 0.1$. Values of f_{spikes} are shown in spikes per iteration, therefore, the value $f_{\text{spikes}} = 0.02$ corresponds to the frequency 40 Hz.

adaptation in linearizing the $f(I)$ curve for RS neurons was proposed in some theoretical works (Ermentrout, 1998; Wang, 1998).

Next we show the behavior of model neurons coupled with chemical synapses. Fig. 5A displays properties of excitatory and inhibitory postsynaptic potentials (EPSP and IPSP) simulated with HH models of cortical neurons. In a pair of RS spiking neurons connected unidirectionally through an AMPA-mediated synapse, a single presynaptic spike induced a postsynaptic EPSP, which can lead to an action potential (see Fig. 5A1). Another common cortical circuit includes reciprocally connected RS and FS neurons. In such a pair, a presynaptic spike in a RS neuron induced an action potential in the FS interneuron that, in turn, induced an IPSP in the RS cell (see Fig. 5A2).

Responses generated in the same networks of neurons, but modeled with the map-based models are shown in Fig. 5B1 and B2, respectively. Despite the simplicity of these models, they capture the main properties of EPSP/IPSP dynamics correctly. The waveforms are plotted for three different strengths of the excitatory synapse to show that the latency of the action potential produced by the postsynaptic neuron was reduced as the synapse strength increased. Note that a small synaptic delay has been explicitly included into the model to achieve a realistic timing of pre- and postsynaptic spikes. The firing of FS interneuron inhibited the postsynaptic RS neuron. The shape of the IPSP is controlled by the parameters of the GABA_A synapse, γ and g_{syn}, of the model (7). The shape of spike afterhyperpolarization (AHP) in the map-based model of a FS interneuron is controlled by the parameters γ^{hp} and g^{hp} see Eq. (5). Therefore, due to the inhibition and AHP effect both neurons remain temporally hyperpolarized after the action potential is triggered in the interneuron.

One-Dimensional Network of Neurons

To illustrate the potential of map-based models in the studies of network activity, we compare the behavior of one-dimensional networks of synaptically connected cortical neurons in HH and map-based simulations. For the sake of simplicity, the inhibitory interneurons were removed from the network. The AMPA mediated synapses were introduced only between the nearest PY (RS type) neurons ($L_{\text{PY}-\text{PY}} = 1$). In the HH model (Fig. 6, left panel), external stimulation initiated burst of activity propagating through the network with constant velocity depending on the strength of synaptic coupling. Such activity has been measured *in vivo* (Timofeev et al., 2000; Topolnik et al., 2003), in disinhibited neocortical slices maintained *in vitro* (Chervin et al., 1988; Chagnac-Amitai and Connors, 1989) and has been described with ODE-based computational models (Golomb and Amitai, 1997; Timofeev et al., 2000; Golomb and Ermentrout, 2001; Bazhenov et al., 2002; Houweling et al., 2002). Here, the increase of intracellular Ca^{2+} concentration over the response duration activated the Ca^{2+} dependent K^+ current that eventually terminated the burst.

Map-based models of RS cells (3) connected in the same network using simple synaptic models (7) demonstrated dynamics very similar to the chain of HH model neurons (compare left and right panels in

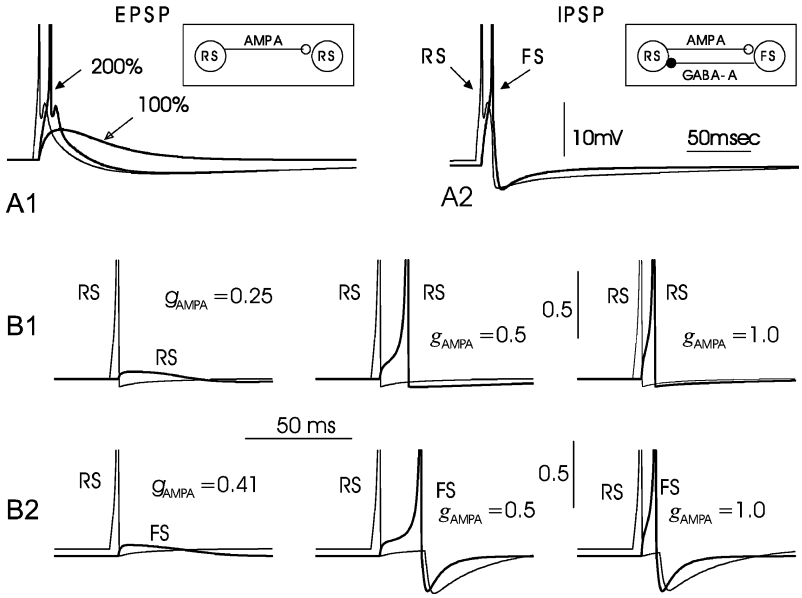

Figure 5. Synaptic potentials in modeled neurons. (A) Hodgkin-Huxley based model. (A1) An action potential in a presynaptic neuron induced an EPSP when delivered through an AMPA-mediated synapse with 100% conductance strength. A spike occurred in the postsynaptic cell when the maximal conductance was increased to 200%. (A2) Reciprocal pair of RS-FS cells. A spike in the presynaptic RS neuron induced an action potential in the postsynaptic FS interneuron followed by an IPSP in the RS neuron. (B) Map-based model. (B1) Two RS neurons ($\alpha = 3.65$, $\sigma = 6.0$E–2, $\mu = 0.0005$, $\sigma^e = 1.0$, $\beta^e = 0.133$) coupled unidirectionally with an excitatory synapse. The parameters of the synapse map were $x_{rp} = 0.0$ and $\gamma = 0.6$. Three different strengths of the synapse $g_{\rm syn} = g_{\rm AMPA}$ are shown. An external stimulus was used to induce a spike in the presynaptic RS neuron. (B2) A presynaptic RS neuron excited a FS neuron, which sent a feedback IPSP to the RS neuron. The parameters of the FS neuron were $\alpha = 3.80$, $y_{\rm rs} = -2.9$, $\gamma^{hp} = 0.85$, $\beta^{hp} = 0.5$ and $g^{hp} = 0.27$. The parameters of the inhibitory synapse ($\rm GABA_A$) were $x_{rp} = -1.1$, $\gamma = 0.96$, and $g_{\rm syn} = 5.0$. The parameters of the excitatory synapse were $x_{rp} = 0.0$, $\gamma = 0.6$ and the time delay was 2 msec. Three different values of $g_{\rm syn} = g_{\rm AMPA}$ are shown.

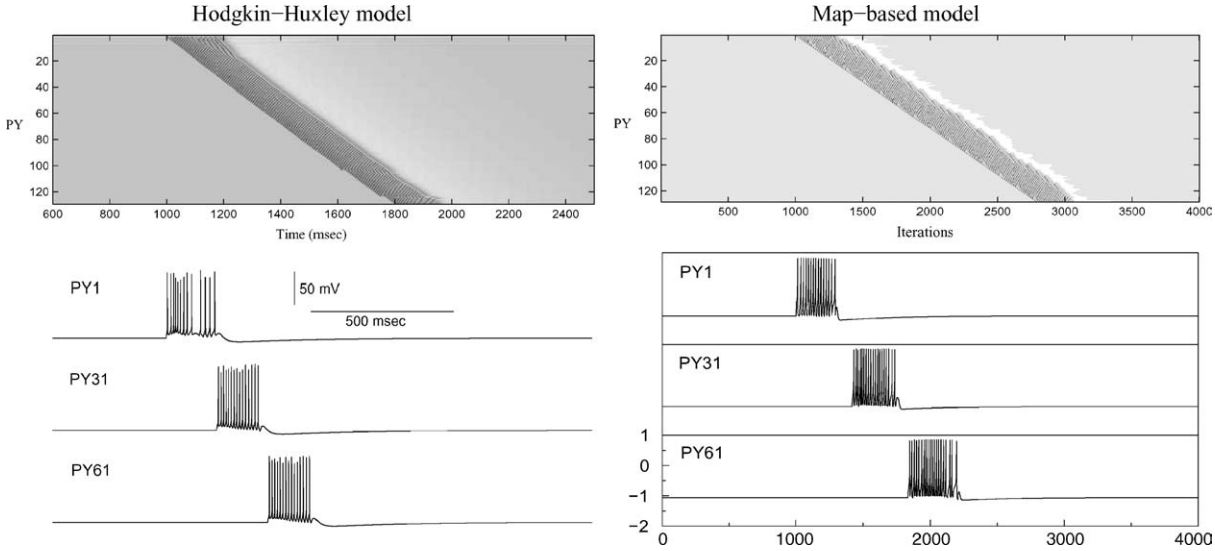

Figure 6. Wave of activity in a one-dimensional chain of excitatory coupled PY (RS type) neurons. No synaptic depression is included. (A) Hodgkin-Huxley model. (B) Map-based model ($g_{\rm syn} = 0.85$). The parameters of the map-based models for the RS neuron and the AMPA synapses are the same as in Fig. 5. External stimulation of cell #1 initiated a burst of activity maintained by lateral PY-PY excitation and the persistent sodium current. Progressive activation of the Ca^{2+} dependent K^+ current terminated the activity in each site. Note that an iteration of the map-based neuron is about 0.5 msec of the HH model.

Fig. 6). The similarity between the dynamics of these model networks is persistent in a wide range of parameter values for the synaptic couplings. It is especially important that the bursts in both of these systems are terminated as a result of intrinsic properties of the neuron dynamics. Note that the effect of synaptic depression was not included in both the HH and the map-based model simulations on purpose to illustrate the role of individual dynamics of the cells in the formation of realistic responses.

Here, we would like to emphasize the computational efficiency of map-based models versus the HH models. The numerical simulation of 2.5 sec of wave propagation in the chain of 128 neurons modeled with HH equations (see Fig. 6, left panel, where that last 1.9 sec are shown) took approximately 9.5 min of CPU time (with an AMD Athlon Processor 1.6 GHz, 1 GB RAM, Linux, GCC 3.2). The simulations of the same network, but modeled with maps, took only 281 msec of CPU time (with an AMD Athlon Processor 1.4 GHz, 512 MB RAM, Windows 2000, Fortran 4.0). The results presented in the right panel of Fig. 6 were computed for a total of 6000 iterations, where only the 4000 last iterations are shown. We studied the consumption of CPU time as a function of the size of the map-based model chain computed for 6000 iterations. The results show that simulation of 256 cells took 551 msec. The simulation time grew linearly with the increasing number of cells in the network and reaches 18 min 47 sec for the case of 131072 cells. This linear growth sustains only if the radius of synaptic connections is kept the same. If the number of presynaptic neurons increases with the size of the array, then the speed of simulations will reduce faster. We should also note that the results of HH simulations shown in the Fig. 6 could be obtained using a reduced set of ionic currents. Some other one-compartmental models could also be used to simulate burst propagation (see, e.g., Golomb and Amitai, 1997; Golomb, 1998). Using these models would speed up HH based simulations. Still we expect them to be orders of magnitude slower than map-based simulations. Numerical simulations of networks containing hundreds of thousands of synaptically coupled cells become quite feasible when the map-based models are used for the description of each neuron.

Velocity of the Wave Fronts and Front Modulation

To explore effects of synaptic interconnections on the properties of propagating waves, we simulated a more complex map-based network model including a layer of RS pyramidal cells and FS interneurons. Similarly to the simplified network model shown in the Fig. 6, a stimulus triggered a wave of spiking activity propagating with constant velocity and terminated by the inhibition mediated by the interneurons (Fig. 8A). The balance of excitation and inhibition controlled the velocity of the wave front propagation (Fig. 7). The direct increase of excitation between RS cells increased the

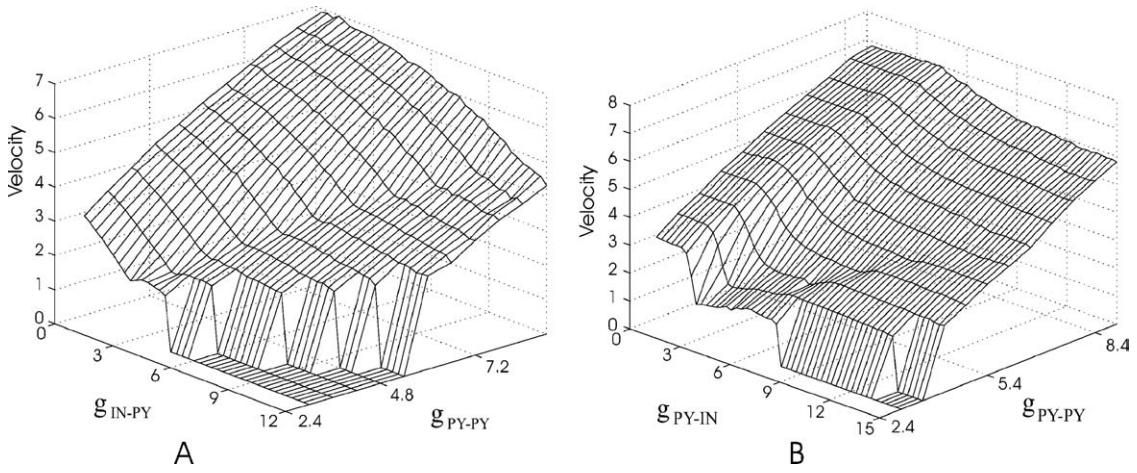

Figure 7. Velocity of the wave front propagation of an excitation burst in the two-layer network as a function of the coupling parameters. (A) $g_{\mathrm{PY-IN}} = 6$ and (B) $g_{\mathrm{IN-PY}} = 4.2$. $L_{\mathrm{PY-PY}} = L_{\mathrm{PY-IN}} = 50$ and $L_{\mathrm{IN-PY}} = 12$. The units of the velocity are given in sites per iteration.

velocity while an increase in feedback through the inhibitory circuits (RS→FS→RS) in general decreased the velocity of wave propagation. The same effects were previously shown with Hodgkin-Huxley based simulations (Bazhenov et al., 2002).

Our analysis has shown that the increase of excitation from RS to FS ($g_{\mathrm{PY-IN}}$) has three stages in the velocity change: (1) at low values of $g_{\mathrm{PY-IN}}$ the velocity did not change with the coupling because interneurons were silent or fired later then the RS cells located within the inhibition footprint; (2) as the coupling increased the interneurons fired earlier, started to inhibit the RS cells before they fired a spike and the velocity decreased rapidly. These two stages are in agreement with known results obtained with HH type models (Bazhenov et al., 2002). (3) With a further increase of the coupling the velocity was stabilized or even grew.

The third stage is a new effect, which we found in the simulations with map-based models. The simulations have shown that this new effect is connected with an instability of the wave front propagation that leads to the onset of periodic variations of the velocity (velocity modulation), see Fig 8B. After the detailed analysis of the parameter balance between the strength of excitation and inhibition that caused the onset of such a modulation we were able to find the same effect in the simulations of the network with HH type models, see Fig. 8C.

In the HH model the wave front modulation typically became apparent only after some initial transient phase and with a sufficiently large footprint of PY to PY connectivity. As the result, a sufficiently large 1D network was required to observe this phenomenon. This and the fact that velocity modulation in both models was found in a relatively narrow region of parameters (near the point where an increase of IN-PY inhibition made wave propagation impossible), can explain why the velocity modulation was not previously observed in HH models. Wave propagation in 1D two-layer networks was explored in great details using integrate-and-fire (IF) based models (see, e.g. Golomb and Ermentrout, 1999, 2002). This study describes two different types of wave propagation: continuous pulses and lurching waves (Golomb and Ermentrout, 2001). In the later case relatively small clusters of neurons fired almost simultaneously and there was significant delay in activation times between neighbor clusters. While the spatio-temporal pattern of lurching waves has some similarities with the wave front modulation described in our work, we believe that the wave modulation is a

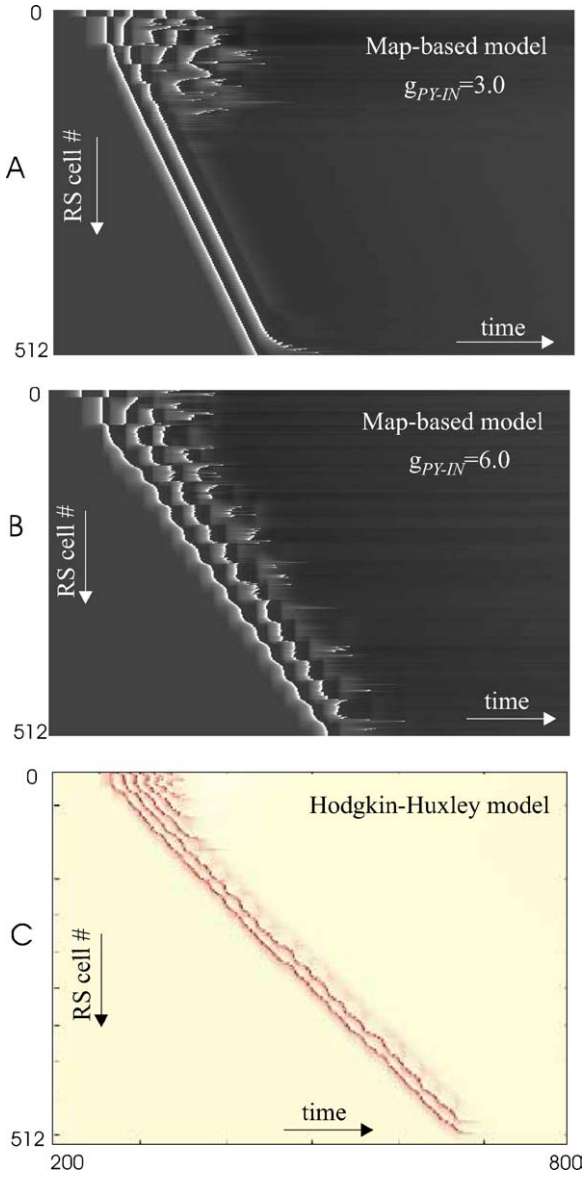

Figure 8. Propagation of the wave front of excitation in a one-dimensional two-layer model of interconnected PY (RS type) and IN (FS type) neurons. (A) and (B) present the map-based model computed for 500 iterations. (A)- propagation with constant velocity ($g_{\mathrm{PY-PY}} = 5.4$, $g_{\mathrm{PY-IN}} = 3.0$, $g_{\mathrm{IN-PY}} = 6.0$). (B) periodic modulation of the wave front velocity ($g_{\mathrm{PY-PY}} = 5.4$, $g_{\mathrm{PY-IN}} = 6.0$, $g_{\mathrm{IN-PY}} = 6.0$). The radii of the connection footprints are 100 RS cells. (C) Front modulation in the Hodgkin-Huxley based network model. The two-layer network included 512 RS and 128 FS neurons. The connection fan out in the HH based model was 12 neurons for RS-RS AMPA mediated synapses, 12 neurons for FS → RS $\mathrm{GABA_A}$ mediated synapses and 3 neurons for RS → FS AMPA mediated synapses. Each neuron was modeled by two compartments including I_{Na}, I_{K}, $I_{\mathrm{Na(p)}}$, I_{Ca}, I_{KCa}, I_{Km}.

different phenomenon since there is no intermediacy in the wave front which is typical for lurching waves (Golomb and Ermentrout, 2001).

Transient and Self-Sustained Dynamics in Large-Scale 2D Network

Only transient waves or persistent activities are possible in one-dimensional networks. Increasing the network dimensionality may lead to new dynamics that include self-sustained rotating spiral waves. A two-dimensional network of sufficiently large size may be required to maintain this activity. The need of a large network for the onset of spiral wave activity was previously demonstrated in a HH based model of isolated thalamic reticular nuclei (Bazhenov et al., 1999). Here we confirmed this finding using a two-layer map-based model of the cortex (Fig. 9). In a small 2D network an external stimulation triggered a quasi-plane wave which propagated through the network similar to the wave of excitation in the 1D network (Fig. 9A, left). As the size of the 2D network grew, the transient plane waves bifurcated into self-sustained spiral waves (Fig. 9A, middle and right). In these simulations the critical network size (the number of neurons) that was required for the onset of self-sustained activity depended on the footprint size of synaptic interconnections. Near the transition point the network dynamics was usually dominated by a single spiral wave moving randomly around the network. Given that open (flow) boundary conditions were used, the spiral wave disappeared when the spiral core reached one of the boundaries, and the network switched to the silent state. However, further increase of the network size resulted in the onset of more stable multi-spiral regimes (Fig. 9A, right). Increasing the network size thus increases the likelihood that self-sustained activity will persist in the network indefinitely.

The properties of the waves in the 2D network were affected by the coupling parameters. An increase of the AMPA mediated coupling between PY neurons extended duration of the bursts and eventually lead to a regime where prolonged up (active) states were interrupted by relatively short down (silent) states. This is illustrated in Figs. 9B and 10A. Figure 9B shows snapshots of the RS cells activity in the network for 3 different values of the excitatory coupling; Fig. 10A displays voltage traces from 2 nearby RS cells and the average activity of 100 (10×10) cells in the center of the network for the regime shown in Fig. 9B (right panel). Here we would like to emphasize that the transitions between up and down states of this activity were not initiated by any external stimuli. These transitions were the result of the intrinsic network dynamics. This network behavior is reminiscent of slow wave sleep oscillations—a periodic (<1 Hz) activity found during natural sleep or under anesthesia (Steriade et al., 1993a, 1993b, 2001; Timofeev et al., 2001b).

A reduction of the inhibitory feedback in the network either by reducing the PY-IN excitation or IN-PY inhibition led to an increase in burst duration. Since the wave front duration sets the spatial scale of a system, the increase of burst duration is equivalent to a reduction of the networks effective size. Therefore, these changes of synaptic strength decreased the maximal number of co-existing waves accommodated in the network, thus increasing the likelihood of a sudden termination of self-sustained activity. This effect is illustrated in Fig. 11 that shows an intensity plot of action potentials for a row of RS neurons (the row which is situated at the center of the 2D network) and the voltage trace of a RS neuron located in the center. These plots show the network dynamics starting at the moment of time when the IN-PY inhibition in the network with stable self-sustained oscillations was reduced from $g_{\mathrm{IN-PY}} = 0.1\ \mu\mathrm{S}$ to $g_{\mathrm{IN-PY}} = 0.05\ \mu\mathrm{S}$ (at time $t = 0$).

Depolarization of cells in the network to the level of spontaneous firing was another way to terminate wave dynamics. This was achieved in the model by increasing the parameter σ in the RS neurons. According to the $f(I)$ diagram shown in Fig. 4, the cells start to fire spontaneously for $I_{\mathrm{DC}} > 0.5$. Slightly above this threshold, the wave structure was still observed but was superimposed with spontaneous random activity (Fig. 9C, left). Further depolarization created random states with individual neurons firing constantly (Fig. 9C, middle and right) which is reminiscent of cortical activity in the awake state. Voltage traces of two RS neurons and the average (over 100 RS cells) activity are shown in Fig. 10B. One can see that neurons fired steadily and without synchrony except for brief time periods when synchrony increased transiently.

Qualitatively different states of the network activity shown in Fig. 9 were characterized by distinct correlation properties of the oscillations. Figure 12 (left column) shows the cross-correlations between two RS neurons separated by distance D and evaluated for an interval of time delays t_d from -1000 to 1000 iterations (see Methods). The figure also shows a similar

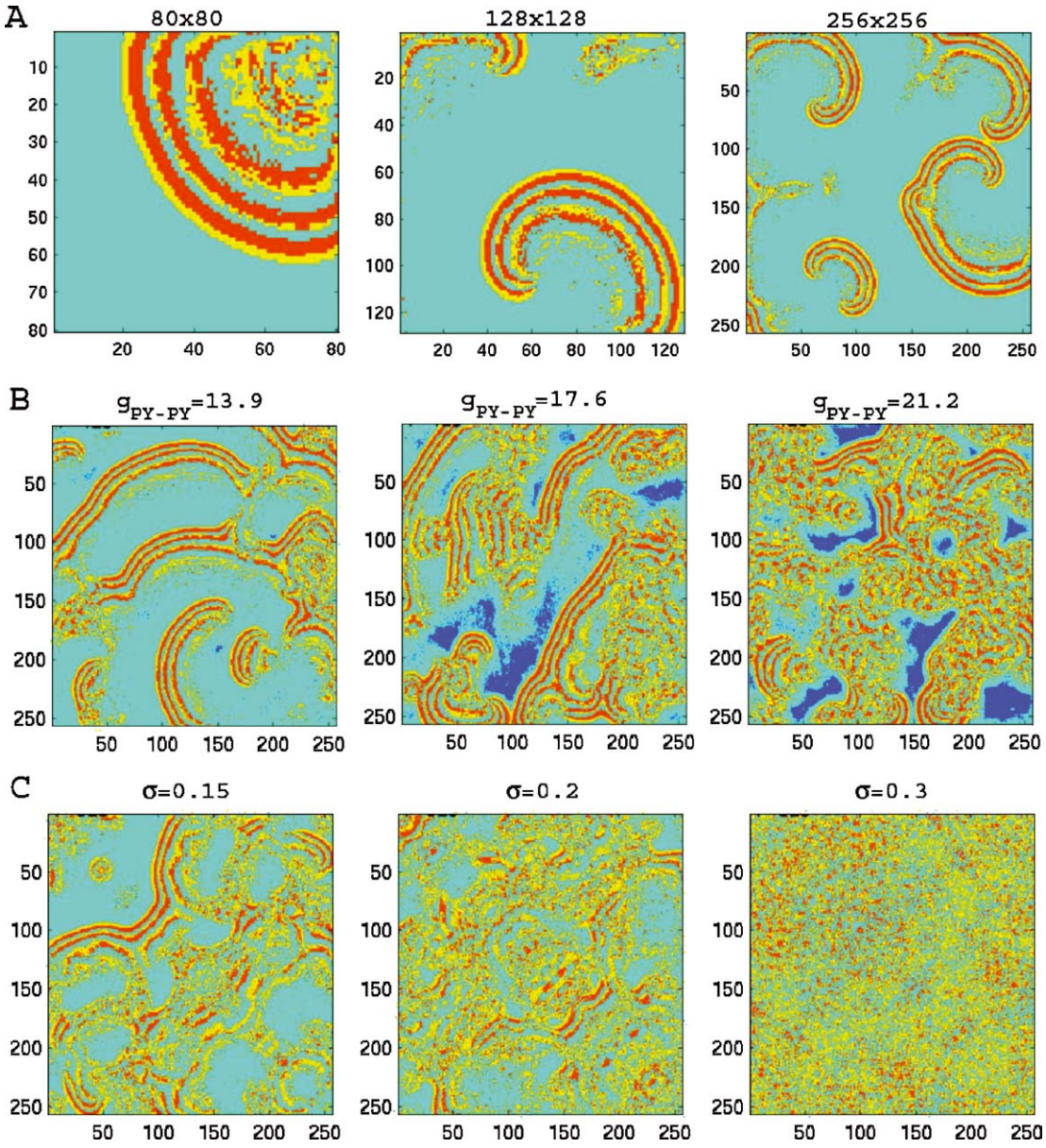

Figure 9. Waves in 2D networks of PY (RS type) and IN (FS type) neurons ($N_{FS} = N_{RS}/4$) coupled through excitatory and inhibitory synapses with short-term depression. (A) Only transient waves were found in a relatively small ($N_{RS} = 6400$) network (left); as the network size increased ($N_{RS} = 25600$, $N_{RS} = 65536$) the bursting activity persisted in a form of rotating spiral waves (middle, right). In all simulations the radius of connection fan out was 8 neurons (∼200 presynaptic neurons) for AMPA mediated RS-RS synapses; 8 neurons (∼200 presynaptic neurons) for AMPA mediated RS-FS synapses; 2 neurons (∼12 presynaptic neurons) for $GABA_A$ mediated FS-RS synapses. (B) An increase of the strength of excitatory coupling between PY neurons transformed the patterns of activity with well separated spirals (left) into the regime dominated by firing cells (right). (C) An increase of the parameter σ depolarized the neurons above the threshold for spontaneous firing. This created an activated network with neuronal behavior similar to the one recorded during waking state or REM sleep.

correlation plots, but computed with the waveforms of the field potential x_n^s in the spots of a footprint of 8×8 cells (right column). For the sake of simplicity we showed the intensity plots of $C(t_d, k, l, k', l')$ measured along a vertical line in the middle of the network, i.e. $k = k'$ and $l = l' + D$.

The main hump of the cross-correlation function centered at $t_d = 0$ and $D = 0$ has specific shapes for

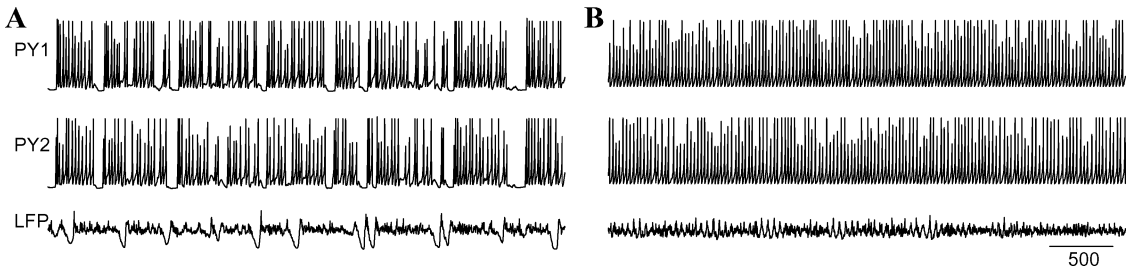

Figure 10. Activities of individual neurons in different network states. (A) Two representative traces of PY cells and averaged network activity (10×10 group in the middle) from the network shown in Fig. 9B, right. A transition between up and down states is similar to activity recorded during slow wave sleep oscillations. (B) "Voltage" traces and averaged activity for the network in the activated state shown in the Fig. 9C, right. The network displays brief epochs with transient increase in coherence.

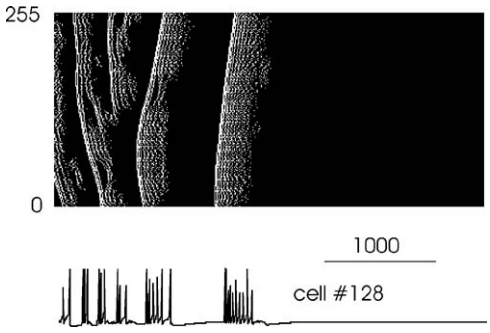

Figure 11. Termination of self-sustained wave dynamics caused by the reduction of inhibition $g_{\text{IN-PY}}$ in the 2D network. The time evolution for a line of RS cells is shown in the intensity plot. The reference time interval is in iterations, where $1000 \sim 500$ msec.

these three cases. In Fig. 12A (narrow waves, Fig. 9A, right), it is wide in both directions (delay and distance) and periodically modulated. In Fig. 12B (wide waves, Fig. 9B, right) it has an extended shape along the coordinate D. In these two cases the correlation in space is caused by the presence of synchrony along wavefronts.

In the case shown in Fig. 12C (active state, Fig. 9C, right) the hump is very sharp in both t_d and D directions. Fast decay of the cross-correlations with a distance between RS neurons found upon network depolarization (Fig. 12C, left) is typical for activated states, which are characterized by minimal correlations of the spike discharges of neighboring neurons (Noda and Adey, 1970). Although the peak of the cross-correlation function in this case is very sharp, the fluctuations of the function at low levels of correlation revealed interesting structure, which can be clearly seen on the plot computed for the averaged signals. This structure appeared as a wide cloud that is periodically modulated in t_d with frequency, at about 40 Hz (Fig. 12C, right). This frequency structure occurred due to occasional increases in spiking synchrony within local groups of neurons. This effect is clearly seen with the analysis of power spectra of waveforms presented in Fig. 13. The left panels of this figure show zoomed fragments of activity in a representative RS cell and averaged activity in a group of 100 RS cells. The power spectra of these activities are shown in the right panel. One can see that although the oscillations in a single RS cell may look almost periodic in the left panel, the power spectra of these oscillations distributed over a range of frequencies and do not have any sharp peaks. At the same time power spectra for the traces of the field potential (averaged activity over 100 RS cells) contains a very sharp peak in the range of 40–45 Hz.

Discussion

Currently the most realistic approach for the simulation of neuronal behavior is based on HH type modeling (Hodgkin and Huxley, 1952). With this approach each ionic current is described with voltage-dependent opening and closing rates for the gating variables. Knowing these rate functions for all currents found for a particular cell type allows one to describe the neuron behavior precisely. However, only very few cell types (e.g., LP neuron of stomatogastric ganglion (STG) system (Golowasch and Marder, 1992)) have been described in detail. The most common computational approach involves the simplification of a neuron model to one or two compartments and the use of the minimum set of ionic currents required to reproduce particular features of neuronal behavior. Examples of successful HH type models based on this reduced approach include

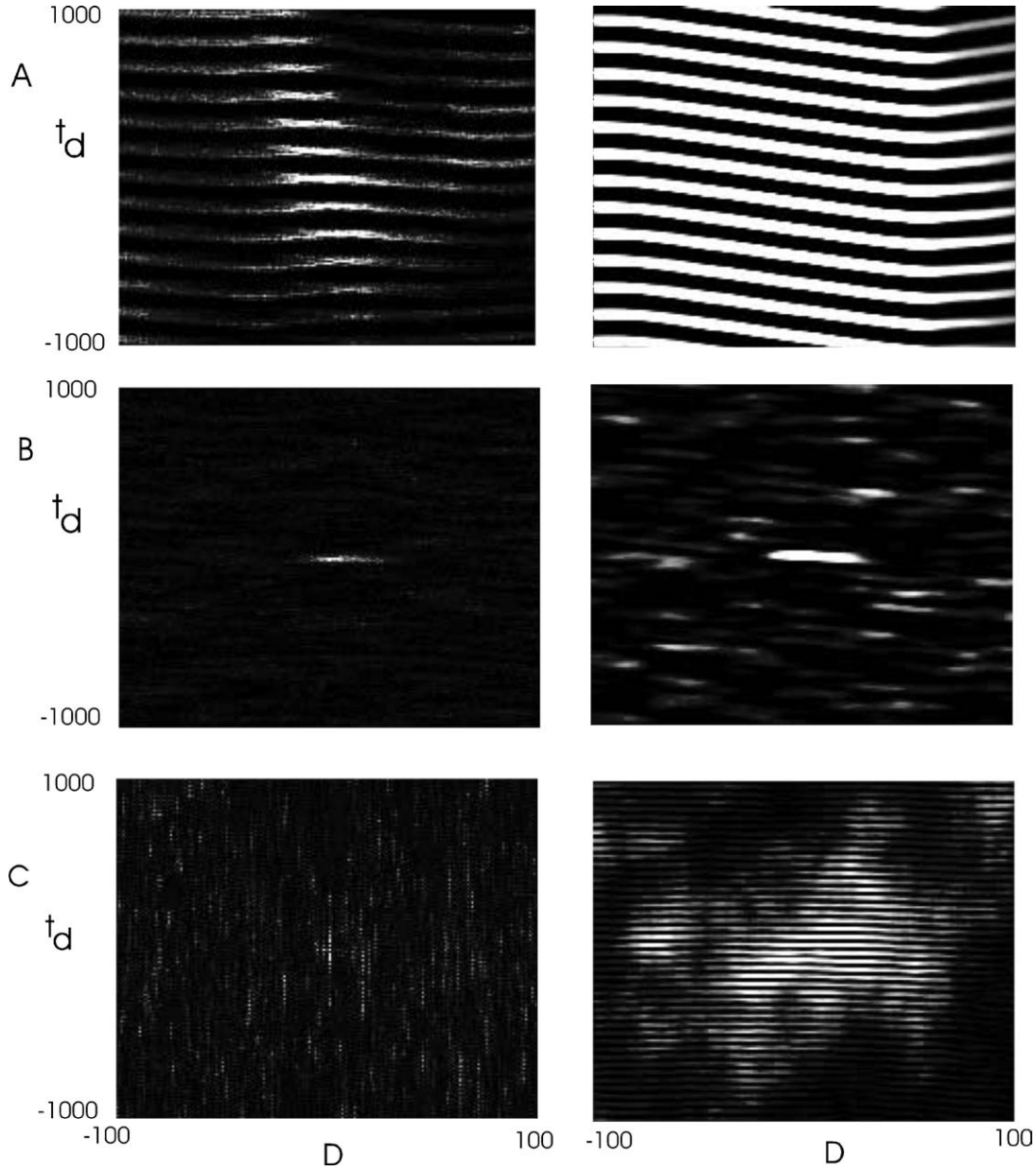

Figure 12. Cross-correlation $C(t_d, k, l, k'l')$ of activities in two neurons (left column) and two spots of 64 neurons (right column) located at $k = k' = l = 125$ and analyzed as a function of distance $D = l' - l$ and delay time t_d. Three distinct cases of network activity are shown: (A) state of multiple spiral waves considered in Fig. 9A right; (B) corresponds to Fig. 9B, right; (C) corresponds to Fig. 9C right. Values of t_d are given in iterations, 1000 iterations correspond to 500 msec.

cortical cell (Mainen and Sejnowski, 1996; Golomb and Amitai, 1997; Golomb, 1998; Bazhenov et al., 2002; Houweling et al., 2002), thalamic relay (Destexhe et al., 1996; Bazhenov et al., 1998, 2000) and reticular (Destexhe et al., 1994a, 1996; Bazhenov et al., 1999) cells, hippocampal neurons (Traub et al., 1996, 1997), antennal lobe neurons (Bazhenov et al., 2001a, 2001b), and many other models. Unfortunately, the high dimensionality and complexity of the nonlinear functions of HH models hamper their application in the simulation of large-scale networks containing a realistic number of neurons.

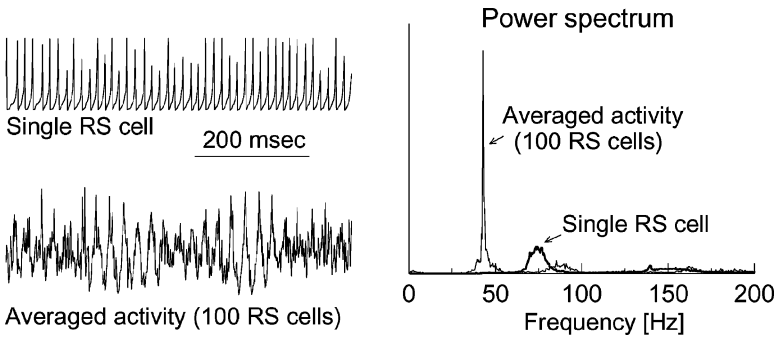

Figure 13. Oscillations in the map based network model. Fragments of the traces from Fig. 10B present the individual oscillations of one RS cell and the averaged activity over a group of cells in the network state shown in Fig. 9C ($\sigma = 0.3$). The power spectra of such traces averaged over 100 RS cells show a sharp peak of power at relatively low frequencies of the field potential (40–45 Hz), right panel.

Another class of models, commonly used when large-scale simulations are needed, is integrate and fire (IF) models (Stein, 1967; Knight, 1972a; Tuckwell, 1988). In the IF model a neuron simply integrates its inputs and generates a spike when a threshold is reached. After the spike, the membrane voltage is reset to zero. This is followed by a refractory period in which spiking is impossible. The disadvantage of IF models is that the firing patterns are oversimplified and do not describe the range of experimental data. Generalizations of this simple model include leaky IF models that introduce a leak term in the dynamics of the subthreshold membrane voltage and integrate-and-fire-or-burst neuron models that reproduce rebound bursting observed in some cell types (Smith et al., 2000; Casti et al., 2002). These IF models have been successfully applied to model firing behavior of the *Limulus* eye neurons (Knight, 1972b), α-motoneurons (Calvin and Stevens, 1968), neurons in the visual system of the housefly (Gestrin et al., 1980), cortical neurons (Softky and Koch, 1993; Troyer and Miller, 1997), and thalamic relay neurons (Smith and Sherman, 2002). However, the generalizations of the IF models that help to describe the realistic firing patterns increase the complexity of the IF-based model and reduce the speed of computer simulations. One exception is the recently proposed model by Izhikevich (Izhikevich, 2003) which is designed in the form a two-dimensional system of ordinary differential equations and allows to replicate a variety of firing patterns.

A class of even simpler models includes phase oscillators (Hoppensteadt and Izhikevich, 1996, 1998; Crook et al., 1997; Williams and Bowtell, 1997; Sigvardt and Miller, 1998; Corchs and Deco, 2001, Ermentrout et al., 2001; Cang and Friesen, 2002), the theta-neuron (Gutkin and Ermentrout, 1998; Longtin et al., 2002) and some other similar models. Those models, however, are not capable of producing a realistic range of experimentally observed firing patterns.

HH based models are preferable in those studies where desirable effects can be obtained in scaled-down network models. For example, thalamic delta (2–3 Hz) oscillations arise as an interplay of a few specific currents (low-threshold Ca^{2+} current (I_T) and hyperpolarization activated cation current (I_h)) and can be studied in a single cell model (Lytton et al., 1996). Thalamic spindle (7–14 Hz) oscillations are a result of interactions between thalamic relay and reticular cells and were successfully studied in models including just a few cells (Destexhe et al., 1994a, 1996; Golomb et al., 1994, 1996; Contreras et al., 1996; Bazhenov et al., 2000; Timofeev et al., 2001a). However, there are dynamical properties, which are observed only in sufficiently large networks. An important example of such dynamics is slow-wave sleep (SWS) oscillations—low-frequency (0.3–1 Hz) rhythms dominating cortical activity during natural sleep and under some types of anesthesia (Steriade et al., 1993a, 1993b, 2001; Timofeev et al., 2001b). Recent studies have reported that slow wave sleep may be essential for memory consolidation and memory formation (Gais et al., 2000; Stickgold et al., 2000). It was proposed that periodic SWS-like network behavior can be observed only if the network of neurons exceeds some large critical size (Timofeev et al., 2000; Bazhenov et al., 2002).

In this study, we developed map-based neuronal models which are capable of reproducing many specific firing patterns observed in different neuronal classes (intrinsically bursting, regular spiking and fast spiking cells). The map-based models can generate more

realistic responses than a conventional IF model, yet it can be simulated much faster than HH-based models. Specific features of a neuron firing patterns (such as effects of AHP, spike adaptation, rebound depolarization, etc.) can be simulated in the map-based model without a decrease of its computational efficiency by setting the proper parameter values. The disadvantage of this approach, however, is that (as opposite to HH-based models) there is no direct relation to the physiological properties of the neuron. The replication of specific firing patterns requires tuning of parameters based upon the phenomenological properties and some patterns may be difficult to reproduce without a significant change of the model equations. Because of the discrete nature of the map-based model, the choice of the time scale is not straightforward and it should be set to be consistent with the time scales of fast and slow dynamics which depend of the other parameters of the map.

The new neuron models were applied to study the collective behavior in one- and two-dimensional network models. In the one-dimensional network model a stimulus created a wave of excitation; its velocity depended on the network parameters (Fig. 7) and this dependence was found to be similar to that previously described using a Hodgkin-Huxley based approach (Bazhenov et al., 2002). A wave propagated through the network and disappeared at the ends of the network. With strong enough inhibitory feedback the inteneurons in the network fired first at the front of the wave in agreement with previous theoretical works (Golomb and Ermentrout, 2002). Plane traveling waves of electrical activity were described in different experimental studies including electrical waves in the olfactory lobe of the terrestrial mollusk *Limax* (Delaney et al., 1994; Kawahara et al., 1997) and in the visual cortex of awake cats (Roelfsema et al., 1997).

Simulations with large scale two-dimensional network models of interconnected RS and FS cells revealed self-sustained dynamics that consisted of interacting spiral waves moving randomly around the network. This behavior was not a function of spontaneously firing cells but a network property and depended on the synaptic interaction between neurons. Dynamical mechanisms responsible for terminating the network activity in particular foci included inhibition that was mediated by local interneurons, spike-frequency adaptation and synaptic depression. Sufficiently large networks supported close to periodic stable dynamics similar to activity found during slow wave sleep. Self-sustained rotating spiral waves mediated by chemical coupling between neurons have been previously described using HH approach (see, e.g., Bazhenov et al., 1999). Thus, two-dimensional network models designed using the map-based approach are capable to replicate complex spatio-temporal patterns found in conductance-based simulations.

The spiral waves described in our study are similar to the ones observed in general reaction-diffusion systems, which may display spiral patterns near the point of bifurcation from spatially-homogeneous solutions (Kuramoto, 1984). One example of spiral wave activity in a biological system is cardiac arrhythmias which are initiated by spiral waves of electrical excitation in heart cells (see, e.g., Winfree, 1987). In this system, however, local electrical coupling is required to maintain spiral waves, which leads to the same mechanism of propagation as in the reaction-diffusion systems. In our cortical network model, the mechanisms promoting pattern formation did not depend on having local interconnections between cells. Experimental support for the existence of rotating spiral waves in neural networks has been provided recently in optical imaging studies of the neuronal activity in turtle visual cortex (Prechtl et al., 1997). A computational model including cortical and thalamic relay neurons was designed to study wave propagation in the turtle visual cortex (Nenadic et al., 2002, 2003). It has been proposed that traveling electrical waves may serve several computational functions including labeling of stimulus features perceived simultaneously with a unique phase (Ermentrout and Kleinfeld, 2001).

Conclusion

The nonlinear maps produce a rich spectrum of dynamical behaviors while remaining simple and low-dimensional systems; they can, therefore, be very computationally efficient. Individual map-based neurons can be connected through conventional chemical and electrical synapses so as to simulate a realistic network structure. The parameters of model can be adjusted to precisely match experimental data. Specific types of thalamic and cortical neurons including thalamic relay and reticular cells, cortical fast spiking, regular spiking, intrinsically bursting and fast-rhythmic-bursting (chattering) neurons can be modeled using this approach. At the same time, the simulations conducted with the map-based model can be orders of magnitude faster than those based on the Hodgkin-Huxley approach.

These results suggest that the new model, which we propose, can be widely used to study diverse processes (such as, e.g., information coding or pattern formation) in large-scale thalamic and cortical networks.

Acknowledgments

This research was supported by grants from NIDCD (M.B.) and Canadian Institutes of Health Research (I.T.). I.T. is scholar of Canadian Institutes of Health Research.

References

Abbott LF, Varela JA, Sen K, Nelson SB (1997) Synaptic depression and cortical gain control. Science 275: 220–224.

Bazhenov M, Stopfer M, Rabinovich M, Abarbanel HD, Sejnowski TJ, Laurent G (2001a) Model of cellular and network mechanisms for odor-evoked temporal patterning in the locust antennal lobe. Neuron. 30: 569–581.

Bazhenov M, Stopfer M, Rabinovich M, Huerta R, Abarbanel HD, Sejnowski TJ, Laurent G (2001b) Model of transient oscillatory synchronization in the locust antennal lobe. Neuron. 30: 553–567.

Bazhenov M, Timofeev I, Steriade M, Sejnowski T (2000) Patterns of spiking-bursting activity in the thalamic reticular nucleus initiate sequences of spindle oscillations in thalamic network. J. Neurophysiol. 84: 1076–1087.

Bazhenov M, Timofeev I, Steriade M, Sejnowski TJ (1998) Computational models of thalamocortical augmenting responses. J. Neurosci. 18: 6444–6465.

Bazhenov M, Timofeev I, Steriade M, Sejnowski TJ (1999) Self-sustained rhythmic activity in the thalamic reticular nucleus mediated by depolarizing GABAA receptor potentials. Nat. Neurosci. 2: 168–174.

Bazhenov M, Timofeev I, Steriade M, Sejnowski TJ (2002) Model of thalamocortical slow-wave sleep oscillations and transitions to activated states. J. Neurosci. 22: 8691–8704.

Calvin WH, Stevens CF (1968) Synaptic noise and other sources of randomness in motoneuron interspike intervals. J. Neurophysiol. 31: 574–587.

Cang J, Friesen WO (2002) Model for intersegmental coordination of leech swimming: central and sensory mechanisms. J. Neurophysiol. 87: 2760–2769.

Casti AR, Omurtag A, Sornborger A, Kaplan E, Knight B, Victor J, Sirovich L (2002) A population study of integrate-and-fire-or-burst neurons. Neural Comput. 14: 957–986.

Chagnac-Amitai Y, Connors BW (1989) Horizontal spread of synchronized activity in neocortex and its control by GABA-mediated inhibition. J. Neurophysiol. 61: 747–758.

Chervin RD, Pierce PA, Connors BW (1988) Periodicity and directionality in the propagation of epileptiform discharges across neocortex. J. Neurophysiol. 60: 1695–1713.

Connors BW, Gutnick MJ (1990) Intrinsic firing patterns of divers neocortical neurons. Trends Neurosci. 13: 99–104.

Contreras D, Destexhe A, Sejnowski, TJ, Steriade M (1996). Control of spatiotemporal coherence of a thalamic oscillation by corticothalamic feedback. Science 274: 771–774.

Corchs S, Deco G (2001) A neurodynamical model for selective visual attention using oscillators. Neural. Netw. 14: 981–990.

Crook SM, Ermentrout GB, Vanier MC, Bower JM (1997) The role of axonal delay in the synchronization of networks of coupled cortical oscillators. J. Comput. Neurosci. 4: 161–172.

Delaney KR, Gelperin A, Fee MS, Flores JA, Gervais R, Tank DW, Kleinfeld D (1994) Waves and stimulus-modulated dynamics in an oscillating olfactory network. Proc. Natl. Acad. Sci. USA 91: 669–673.

Destexhe A, Bal T, McCormick DA, Sejnowski TJ (1996) Ionic mechanisms underlaying synchronized and propagating waves in a model of ferret thalamic slices. J. Neurophysiol. 76: 2049–2070.

Destexhe A, Contreras D, Sejnowski TJ, Steriade M (1994a) A model of spindle rhythmicity in the isolated thalamic reticular nucleus. J. Neurophysiol. 72: 803–818.

Destexhe A, Mainen ZF, Sejnowski TJ (1994b) Synthesis of models for excitable membranes, synaptic transmission and neuromodulation using a common kinetic formalism. J. Comput. Neurosci. 1: 195–230.

Ermentrout B (1998) Linearization of F-I curves by adaptation. Neural Comput. 10: 1721–1729.

Ermentrout B, Wang JW, Flores J, Gelperin A (2001) Model for olfactory discrimination and learning in Limax procerebrum incorporating oscillatory dynamics and wave propagation. J. Neurophysiol. 85: 1444–1452.

Ermentrout GB, Kleinfeld D (2001) Traveling electrical waves in cortex: Insights from phase dynamics and speculation on a computational role. Neuron. 29, 33–44.

Gais S, Plihal W, Wagner U, Born J (2000) Early sleep triggers memory for early visual discrimination skills. Nat. Neurosci. 3: 1335–1339.

Galarreta M, Hestrin S (1998) Frequency-dependent synaptic depression and the balance of excitation and inhibition in the neocortex. Nat. Neurosci. 1: 587–594.

Gestrin G, Masterbroek HAK, Zaagman WH (1980) Stochastic constancy, variability and adaptation of spike generation: Performance of a giantneuron in the visual system of the fly. Biol. Cybern. 38: 31–40.

Golomb D (1998) Models of neuronal transient synchrony during propagation of activity through neocortical circuitry. J. Neurophysiol. 79: 1–12.

Golomb D, Amitai Y (1997) Propagating neuronal discharges in neocortical slices: Computational and experimental study. Journal of Neurophysiology. 78: 1199–1211.

Golomb D, Ermentrout GB (1999) Continuous and lurching traveling pulses in neuronal networks with delay and spatially decaying connectivity. Proc. Natl. Acad. Sci. USA 96: 13480–13485.

Golomb D, Ermentrout GB (2001) Bistability in pulse propagation in networks of excitatory and inhibitory populations. Phys. Rev. Lett. 86: 4179–4182.

Golomb D, Ermentrout GB (2002) Slow excitation supports propagation of slow pulses in networks of excitatory and inhibitory populations. Phys. Rev. E. Stat. Nonlin Soft Matter Phys. 65: 061911.

Golomb D, Wang XJ, Rinzel J (1994) Synchronization properties of spindle oscillations in a thalamic reticular nucleus model. J. Neurophysiol. 72: 1109–1126.

Golomb D, Wang X-J, Rinzel J (1996) Propagation of spindle waves in a thalamic slice model. Journal of Neurophysiology. 75: 750–769.

Golowasch J, Marder E (1992) Ionic currents of the lateral pyloric neuron of the stomatogastric ganglion of the crab. J. Neurophysiol. 67: 318–331.

Gray CM, McCormick DA (1996) Chattering cells: Superficial pyramidal neurons contributing to the generation of synchronous oscillations in the visual cortex. Science 274: 109–113.

Gutkin BS, Ermentrout GB (1998) Dynamics of membrane excitability determine interspike interval variability: A link between spike generation mechanisms and cortical spike train statistics. Neural. Comput. 10: 1047–1065.

Hodgkin AL, Huxley AF (1952) A quantitative description of membrane current and its application to conduction and excitation in nerve. J. Physiol. Lond. 117: 500–544.

Hoppensteadt FC, Izhikevich EM (1996) Synaptic organizations and dynamical properties of weakly connected neural oscillators. II. Learning phase information. Biol. Cybern. 75: 129–135.

Hoppensteadt FC, Izhikevich EM (1998) Thalamo-cortical interactions modeled by weakly connected oscillators: Could the brain use FM radio principles? Biosystems. 48: 85–94.

Houweling AR, Bazhenov M, Timofeev I, Grenier F, Steriade M, Sejnowski TJ (2002) Frequency-selective augmenting responses by short-term synaptic depression in cat neocortex. J. Physiol. 542: 599–617.

Izhikevich EM (2003) Simple model of spiking neurons. IEEE Transactions on Neural Networks. 14: 1569–1572.

Izhikevich EM (2004) Which model to use for cortical spiking neurons? IEEE Transactions on Neural Networks (in press).

Jahnsen H, Llinás R (1984) Electrophysiological properties of guinea-pig thalamic neurones: An *in vitro* study. Journal of Physiology 349: 205–226.

Kawahara S, Toda S, Suzuki Y, Watanabe S, Kirino Y (1997) Comparative study on neural oscillation in the procerebrum of the terrestrial slugs Incilaria bilineata and J. Exp. Biol. 200: 1851–1861.

Knight BW (1972a) Dynamics of encoding in a population of neurons. J. Gen Physiol. 59: 734–766.

Knight BW (1972b) The relationship between the firing rate of a single neuron and the level of activity in a population of neurons. Experimental evidence for resonant enhancement in the population response. J. Gen. Physiol. 59: 767–778.

Kuramoto Y (1984) Chemical oscillations, waves, and turbulence. Springer-Verlag, Berlin–Heidelberg–New York–Tokyo.

Longtin A, Doiron B, Bulsara AR (2002) Noise-induced divisive gain control in neuron models. Biosystems. 67: 147–156.

Lytton WW, Destexhe A, Sejnowski TJ (1996) Control of slow oscillations in the thalamocortical neuron: A computer model. Neuroscience. 70: 673–684.

Mainen ZF, Sejnowski TJ (1996) Influence of dendritic structure on firing pattern in model neocortical neurons. Nature 382: 363–366.

Mason A, Larkman A (1990) Correlations between morphology and electrophysiology of pyramidal neurons in slices of rat visual cortex. II. Electrophysiology. J. Neurosci. 10: 1415–1428.

McCormick DA, Connors BW, Lighthall JW, Prince DA (1985) Comparative electrophysiology of pyramidal and sparsely spiny stellate neurons of the neocortex. J. Neurophysiol. 54: 782–806.

Nenadic Z, Ghosh BK, Ulinski P (2003) Propagating waves in visual cortex: A large-scale model of turtle visual cortex. J Comput Neurosci. 14: 161–184.

Nenadic Z, Ghosh BK, Ulinski PS (2002) Modeling and estimation problems in the turtle visual cortex. IEEE Trans. Biomed. Eng. 49: 753–762.

Noda H, Adey WR (1970) Firing of neuron pairs in cat association cortex during sleep and wakefulness. J. Neurophysiol. 33: 672–684.

Pinsky PF, Rinzel J (1994) Intrinsic and network rhythmogenesis in a reduced Traub model for CA3 neurons. J. Comput. Neurosci. 1: 39–60.

Prechtl JC, Cohen LB, Pesaran B, Mitra PP, Kleinfeld D (1997) Visual stimuli induce waves of electrical activity in turtle cortex. Proc. Natl. Acad. Sci. USA 94: 7621–7626.

Roelfsema PR, Engel AK, Konig P, Singer W (1997) Visuomotor integration is associated with zero time-lag synchronization among cortical areas. Nature 385: 157–161.

Rulkov NF (2002) Modeling of spiking-bursting neural behavior using two-dimensional map. Phys. Rev. E Stat. Nonlin. Soft Matter Phys. 65: 041922.

Shilnikov AL, Rulkov NF (2003), Origin of chaos in a two-dimensional map modeling spiking-bursting neural activity. Int. J. Bif. and Chaos. 13: 3325–3340.

Sigvardt KA, Miller WL (1998) Analysis and modeling of the locomotor central pattern generator as a network of coupled oscillators. Ann. NY Acad. Sci. 86: 250–265.

Smith GD, Cox CL, Sherman SM, Rinzel J (2000). Fourier analysis of sinusoidally driven thalamocortical relay neurons and a minimal integrate-and-fire-or-burst model. J. Neurophysiol. 83: 588–610.

Smith GD, Sherman SM (2002) Detectability of excitatory versus inhibitory drive in an integrate-and-fire-or-burst thalamocortical relay neuron model. J. Neurosci. 22: 10242–10250.

Softky WR, Koch C 1993. The highly irregular firing of cortical cells is inconsistent with temporal integration of random EPSPs. J. Neurosci. 13: 334–350.

Stein RB (1967) The frequency of nerve action potentials generated by applied currents. Proc. R. Soc. Lond B. Biol. Sci. 167: 64–86.

Steriade M, McCormick DA, Sejnowski TJ (1993a) Thalamocortical oscillations in the sleeping and aroused brain. Science 262: 679–685.

Steriade M, Nuñez A, Amzica F (1993b) A novel slow (<1 Hz) oscillation of neocortical neurons *in vivo*: Depolarizing and hyperpolarizing components. J. Neurosci. 13: 3252–3265.

Steriade M, Timofeev I, Dürmüller N, Grenier, F (1998) Dynamic properties of corticothalamic neurons and local cortical interneurons generating fast rhythmic (30–40 Hz) spike bursts. J. Neurophysiol. 79: 483–490.

Steriade M, Timofeev I, Grenier F (2001) Natural waking and sleep states: A view from inside neocortical neurons. J. Neurophysiol. 85: 1969–1985.

Stickgold R, James L, Hobson JA (2000) Visual discrimination learning requires sleep after training. Nat. Neurosci. 3: 1237–1238.

Timofeev I, Bazhenov M, Sejnowski T, Steriade M (2001a) Contribution of intrinsic and synaptic factors in the desynchronization of thalamic oscillatory activity. Thalamus and related systems. 1: 53–69.

Timofeev I, Grenier F, Bazhenov M, Sejnowski TJ, Steriade M (2000) Origin of slow cortical oscillations in deafferented cortical slabs. Cer. Cortex 10: 1185–1199.

Timofeev I, Grenier F, Steriade M (2001b) Disfacilitation and active inhibition in the neocortex during the natural sleep-wake cycle: An intracellular study. PNAS 98: 1924–1929.

Topolnik L, Steriade M, Timofeev I (2003) Partial cortical deafferentation promotes development of paroxysmal activity. Cereb. Cortex 13: 883–893.

Traub RD, Jefferys JG, Whittington MA (1997) Simulation of gamma rhythms in networks of interneurons and pyramidal cells. J. Comput. Neurosci. 4: 141–150.

Traub RD, Whittington MA, Colling SB, Buzsaki G, Jefferys JG (1996) Analysis of gamma rhythms in the rat hippocampus in vitro and in vivo. J. Physiol. 493 (Pt 2): 471–484.

Troyer TW, Miller KD (1997) Physiological gain leads to high ISI variability in a simple model of a cortical regular spiking cell. Neural Comput. 9: 971–983.

Tsodyks MV, Markram H (1997) The neural code between neocortical pyramidal neurons depends on neurotransmitter release probability. Proc. Natl. Acad. Sci. 94: 719–723.

Tuckwell HC (1988) Introduction to Theoretical Neurobiology. Vol. 2, Nonlinear and Stochastic Theries. Cambridge University Press, Cambridge.

Wang XJ (1998) Calcium coding and adaptive temporal computation in cortical pyramidal neurons. J. Neurophysiol. 79: 1549–1566.

Williams TL, Bowtell G (1997) The calculation of frequency–shift functions for chains of coupled oscillators, with application to a network model of the lamprey locomotor pattern generator. J. Comput. Neurosci. 4: 47–55.

Winfree A (1987) When Time Breaks Down. Springer–Verlag, New York.